1992

An Observational Study of Sea- and Land-Breeze Circulation in an Area of Complex Coastal Heating

Shiyuan Zhong
Iowa State University

Eugene S. Takle
Iowa State University, gstakle@iastate.edu

An Observational Study of Sea- and Land-Breeze Circulation in an Area of Complex Coastal Heating*

SHIYUAN ZHONG AND EUGENE S. TAKLE

Department of Geological and Atmospheric Sciences, Department of Agronomy, Iowa State University, Ames, Iowa

(Manuscript received 5 September 1991, in final form 30 June 1992)

ABSTRACT

The diurnal evolution of the three-dimensional structure of a mesoscale circulation system frequently occurring in the area of Kennedy Space Center–Cape Canaveral has been studied using the data from the Kennedy Space Center Atmospheric Boundary Layer Experiment (KABLE). The case was chosen from the spring intensive data-collection period when the greatest daytime temperature difference between land and water (sea and inland rivers) occurs and the local circulations are most intense. The daytime flow structure was determined primarily by the mesoscale pressure-gradient force created by the temperature contrast between land and water. A strong sea-breeze circulation, the dominant feature of the daytime flow field, was modified by a local inland river breeze, known as the *Indian River breeze*, in that divergent flow over the river enhanced the sea-breeze convergence on the seaward side and generated additional convergence on the landward side of the river. The rivers near the coastline also modified the initial flow field by enhancing convergence in the surrounding areas and speeding up the movement of the sea-breeze front. The nighttime flow structure was dominated by a large-scale land breeze that was relatively uniform over the area and became quasi-stationary after midnight. The nonuniformity of the wind-vector rotation rate suggests that mesoscale forcing significantly modifies the Coriolis-induced oscillation. No clear convergence patterns associated with the rivers were observed at night. Detailed characteristics over a diurnal cycle of the sea–land breeze and of the river breeze onset time, strength, depth, propagation speed, and both landward and seaward extension, are documented in this study. Some boundary-layer characteristics needed for predicting diffusion of pollutants released from coastal launch pads, including atmospheric stability, depth of the thermal internal boundary layer, and turbulent mixing, are also discussed.

1. Introduction

The Kennedy Space Center–Cape Canaveral (KSC–CC) area is rich in water–land interfaces. Complex low-level circulation patterns frequently occur in this region, creating concerns for operations in which the atmospheric diffusion of rocket-exhaust effluent or the accidental release of radioactive material to the atmosphere must be considered. Transport of pollutants from coastal launch pads may present several serious problems. One concern is surface fumigation by elevated pollutant plumes brought to the surface as a result of the growth of a thermal internal boundary layer; another is the recirculation of pollutants within mesoscale circulation patterns. These concerns are directly related to the local wind system and stability regimes.

Neumann (1971) outlined some diagnostic tools for forecasting thunderstorm activity and associated adverse weather phenomena at KSC–CC and concluded that the thunderstorm forecasting problem at this site is primarily one of forecasting the low-level wind field and, to a lesser extent, the attendant synoptic-scale convergence–divergence pattern. Hill (1967) and Reed (1979) applied statistical analysis to data from meteorological towers and were able to identify some of the general characteristics of the sea and land breezes in the KSC–CC area. These studies were limited to the tower layer with no significant information about the other regions of the planetary boundary layer (PBL). Lyons et al. (1988) used a mesoscale numerical model to generate guidance products to improve forecasts of sea-breeze-generated thunderstorms in support of space shuttle operations at KSC–CC. Coarse horizontal resolution and lack of consideration of three-dimensional effects, however, precluded model resolution of the small-scale flow structures created by inhomogeneities in surface heating.

The Kennedy Space Center Atmospheric Boundary Layer Experiment (KABLE), a recently completed intensive field observation program in the KSC–CC area, revealed flow structures on scales not previously observed or modeled, including divergence and convergence patterns, river breezes, and sea–land breezes. This four-dimensional dataset provides information not only on details of the local meteorology but also on the fundamental issue of interactions of different mesoscale phenomena. In a previous investigation

* Journal Paper No. J-14637 of the Iowa Agriculture and Home Economics Experiment Station, Ames, Iowa; Project No. 2779.

Corresponding author address: Eugene S. Takle, Department of Geological and Atmospheric Sciences, Iowa State University, 3010 Agronomy Building, Ames, IA 50011.

(Zhong et al. 1991), we simulated the flow structure of a typical day from the fall intensive data-collection period by using a three-dimensional mesoscale numerical model. A simulation with a resolution of 1.5 km revealed the spatial complexity of the wind field at KSC–CC caused by the complex surface-heating pattern and the curved coastline, and also identified the effects of the local rivers and lagoons on the sea-breeze circulation. The current paper presents a case study of observations from the spring intensive data-collection period (26–27 May 1989) for which the synoptic forcing was weak and local circulations dominated the area. It has been observed that local circulations reach their peak at this time of year because the daytime temperature difference between land and water is greatest (Reed 1979). An analysis of the four-dimensional dataset with high resolution near the coast reveals new additional information about the vertical structure and the diurnal evolution of the flow field at KSC–CC.

2. Observations

The KABLE field experiment consisted of an entire year of continuous data acquisition from November 1988 through October 1989 and three short-term intensive data-collection periods during the experiment period. KABLE objectives were to determine not only general features and seasonal characteristics but also the detailed structure of the PBL in the KSC–CC area. Observations were obtained from a variety of in situ and remote sensors. An overview of the KABLE observations and the details of instrumentation are provided by Taylor et al. (1990).

Surface observations for the case studied consisted of data from a coastal buoy, synoptic surface weather stations, satellite imagery of sea surface temperatures, insolation measurement stations, and a network of approximately 48 towers located from along the coastline to slightly more than 40 km inland. The density of stations was high enough to resolve the surface mesoscale circulation patterns over KSC–CC.

In addition to surface observations, there were acoustic sounders at a coastal site and on the west bank of the Indian River, a high-resolution rawinsonde at Cape Canaveral Air Force Station, and synoptic upper-air observations. The observational domain and the locations of instruments are indicated in Fig. 1.

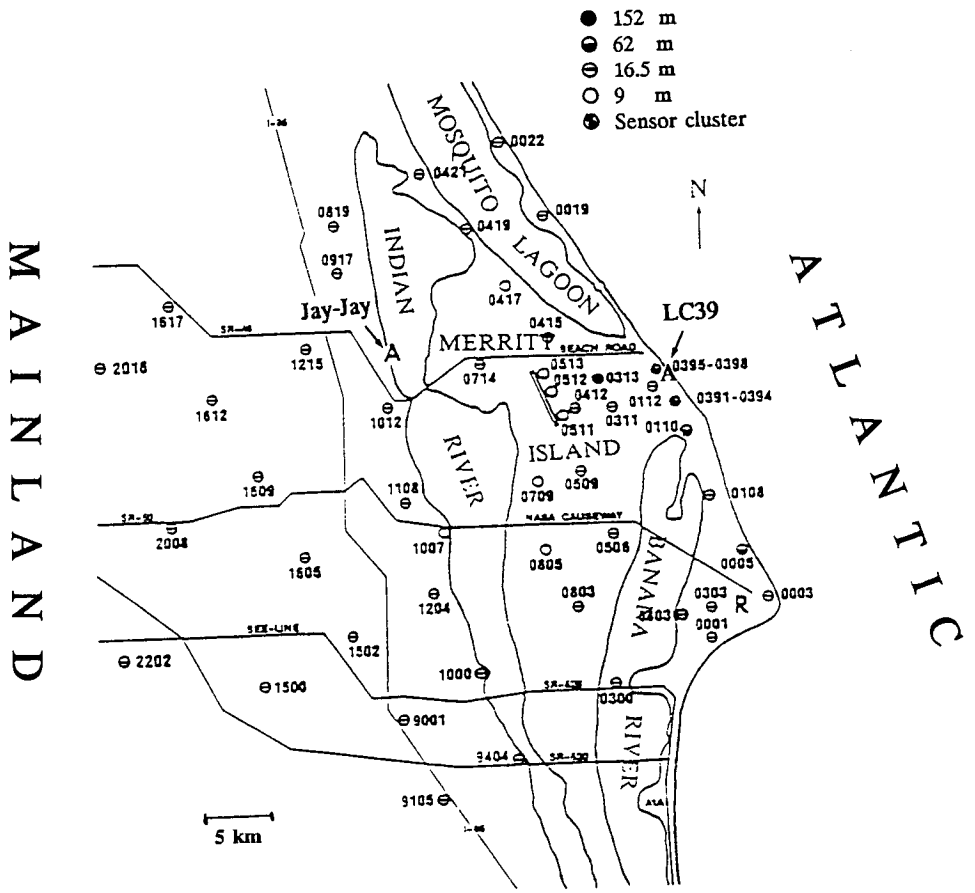

FIG. 1. KABLE area and the key sensor locations. A: acoustic sounders, R: rawinsonde, and circles: instrumented towers.

3. Synoptic overview

Surface and 500-mb maps for the beginning and the ending of the 24-h analysis period are shown in Fig. 2. No major synoptic-scale pressure gradients influenced the flow over Florida except the westward extension of the Bermuda high, which covered the southeastern states, including the KSC–CC area. Weak pressure gradients and light and variable winds were the dominant features of the surface maps over the area of interest for this period. At 500 mb, a high centered over the Gulf of Mexico dominated the region. Upper-level winds were from the north at the beginning and veered slightly during the day to become northeasterly by the end of the study period.

4. Results and discussion

a. Surface temperature distribution

Temperature contrast between land and water bodies is the primary cause for generation of the flow field in

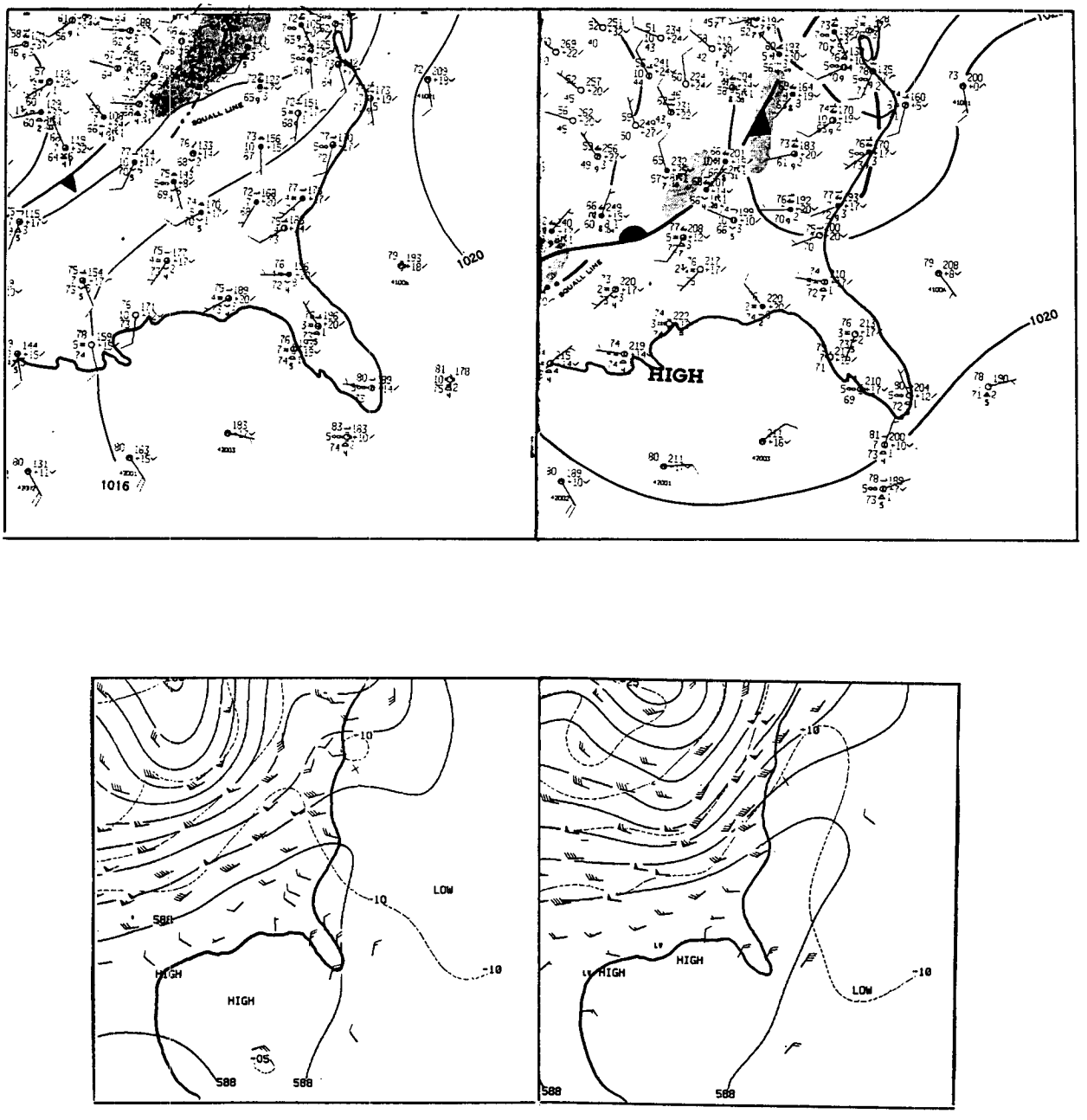

FIG. 2. Surface (top) and 500-mb (bottom) weather maps at 0700 EST, 26 (left) and 27 (right) May 1989.

a situation of weak synoptic forcing. Figure 3 shows the cross-coastline temperature distribution at 28.5°N measured by the *NOAA-11* satellite at 1350 EST 26 May and 0200 EST 27 May. In the afternoon, the Gulf Stream temperature was considerably lower than the inland temperature, and the temperature of inland water was cooler than that of the surrounding land area. At night, however, this temperature distribution was reversed: cool temperatures existed over the land surface, whereas warmer temperatures were reported at locations of the Gulf Stream, the Banana River, and the Indian River. The temperature at Orlando International Airport (MCO) was slightly higher than that of the surrounding area, which might have been caused by the heat-island effect of the city of Orlando.

Figure 4 shows the time rate of change of temperature differences between Orlando International Airport, located about 90 km inland, and data buoy 41009, located 40 km east of the eastern tip of Cape Canaveral. The temperature difference during the day was much higher than that at night. The inland temperature exceeded the Gulf Stream temperature about 2.5 h after sunrise (approximately 0530 EST at KSC–CC). The temperature difference reached its peak value of about 8°C just before 1400 and remained almost steady for the next 3 h before starting to drop. The inland temperature dropped below the water-surface temperature about 2 h after sunset (1910 EST), and differential cooling dominated until morning. The maximum value of the nighttime temperature difference was less than 3°C, in contrast to a daytime difference of about 8°C. A stronger thermal forcing is, therefore, expected during the daytime than the nighttime.

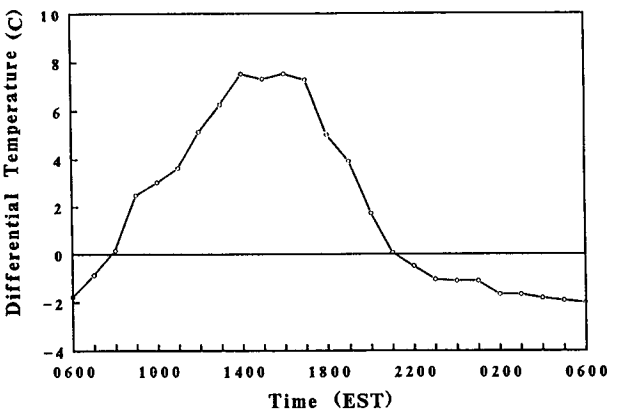

FIG. 4. Diurnal evolution of the temperature difference between MCO and data buoy 41009.

b. *Flow field*

Observed winds at 16.5 m, shown in Fig. 5 at 2-h intervals, reveal the horizontal structure of the wind field. Examination of this set of plots suggests that the flow patterns may be classified as daytime or nighttime regimes. The daytime regime prevailed from sunrise to sunset and was characterized by flow from northwest through east. The nighttime regime, in contrast, was characterized by southeast–southwest flow.

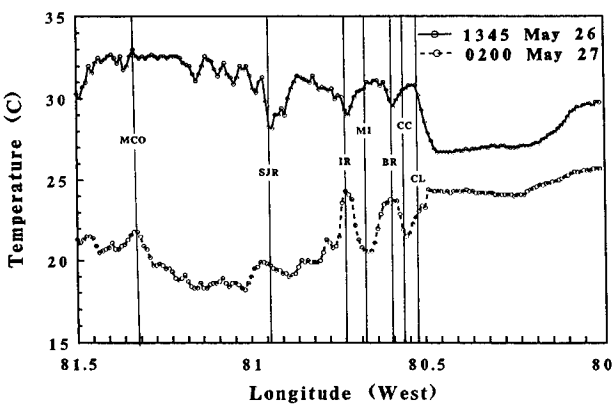

FIG. 3. Surface temperature distribution at 28.5°N. MCO = Orlando International Airport, SJR = St. John's River, IR = Indian River, MI = Merritt Island, BR = Banana River, CC = Cape Canaveral, and CL = coastline.

In the early morning of 26 May, the prevailing wind was northwest offshore at 1–2 m s^{-1}, except at the northern coastline east of Mosquito Lagoon where a wind speed of 3.6 m s^{-1} was observed. A sea breeze developed at the coast approximately 3 h after sunrise, as indicated at 0900 EST by a shift in wind direction from northwest offshore to northeast onshore and an increase in wind speed at the coast. River breezes also developed at the same time, as indicated by the divergent flows over the inland water bodies (the rivers and lagoons). Two convergence centers, one at the center of Merritt Island and the other between the coast and the Banana River, and a weak convergence zone west of the Indian River were therefore formed as a result of the wind shift. By 1100, the sea-breeze front passed Mosquito Lagoon in the northern part of the region, the Banana River in the southern part, and most of Merritt Island, reaching the east bank of the Indian River. The divergence patterns over the Banana River and Mosquito Lagoon were suppressed by the sea-breeze onshore flow before developing relatively strong river breezes. Meanwhile, the divergent flow over the Indian River was strengthening and formed a relatively strong river breeze called the *Indian River breeze* (IRB). The wind speed in the area of the sea breeze was 3–5 m s^{-1}, whereas the wind speed in the area of IRB was less than 3 m s^{-1}. This is because the surface-heating contrast between the Indian River and the surrounding land area was weaker than that between sea and land.

Patterns of wind direction and wind speed on both sides of the Indian River became relatively uniform by 1300, indicating that the sea breeze had passed the river

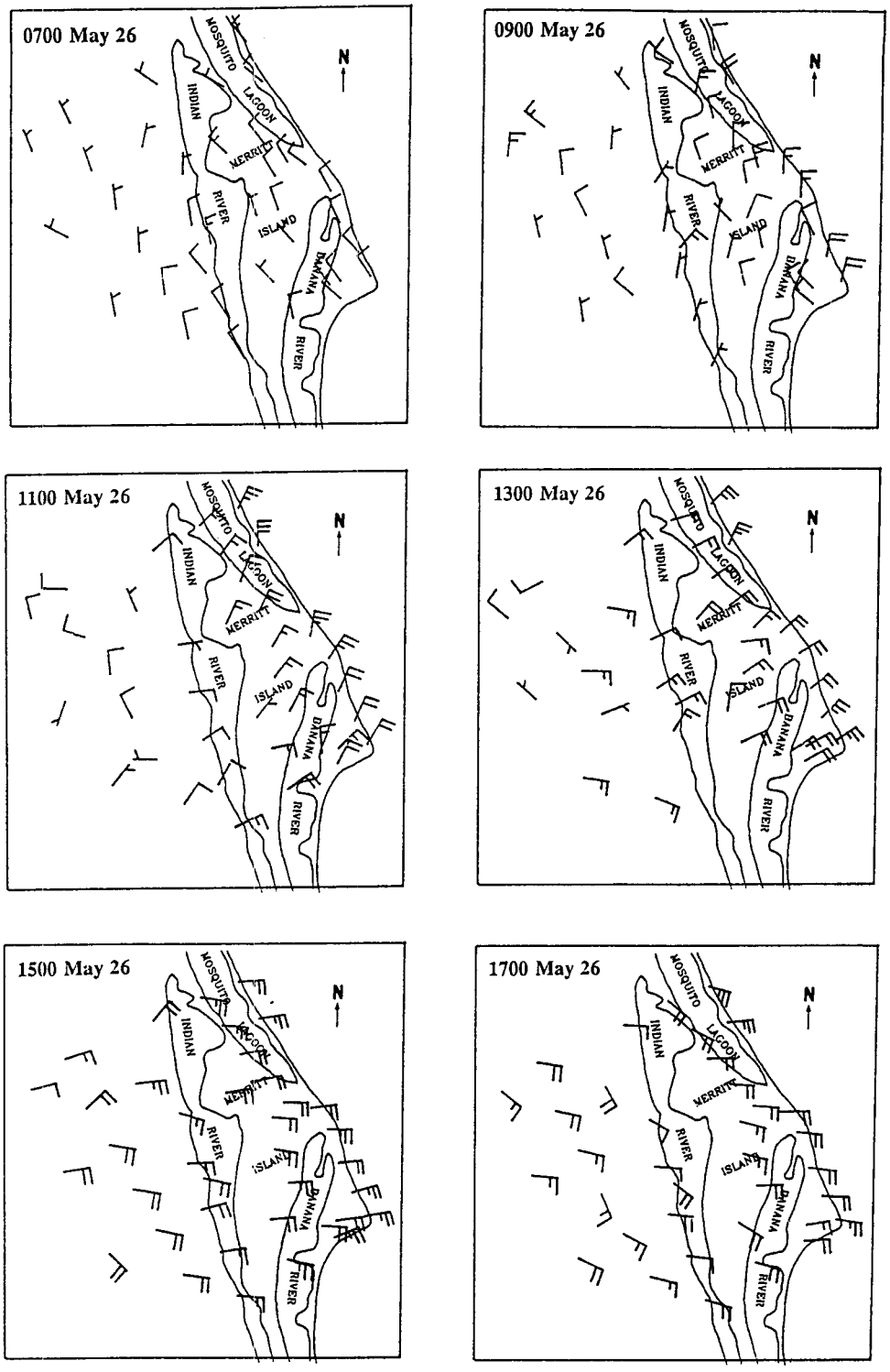

FIG. 5. Horizontal wind field at 16.5 m measured by the tower network. Units: half-barb is 1 m s^{-1} and full barb is 2 m s^{-1}.

and merged with the IRB west of the Indian River. By 1500, onshore flow existed everywhere from the coast to more than 40 km inland at the westernmost tower. The average speed of sea-breeze inland penetration measured by the tower network was about 2 m s^{-1}, which was about twice the speed of the IRB before they

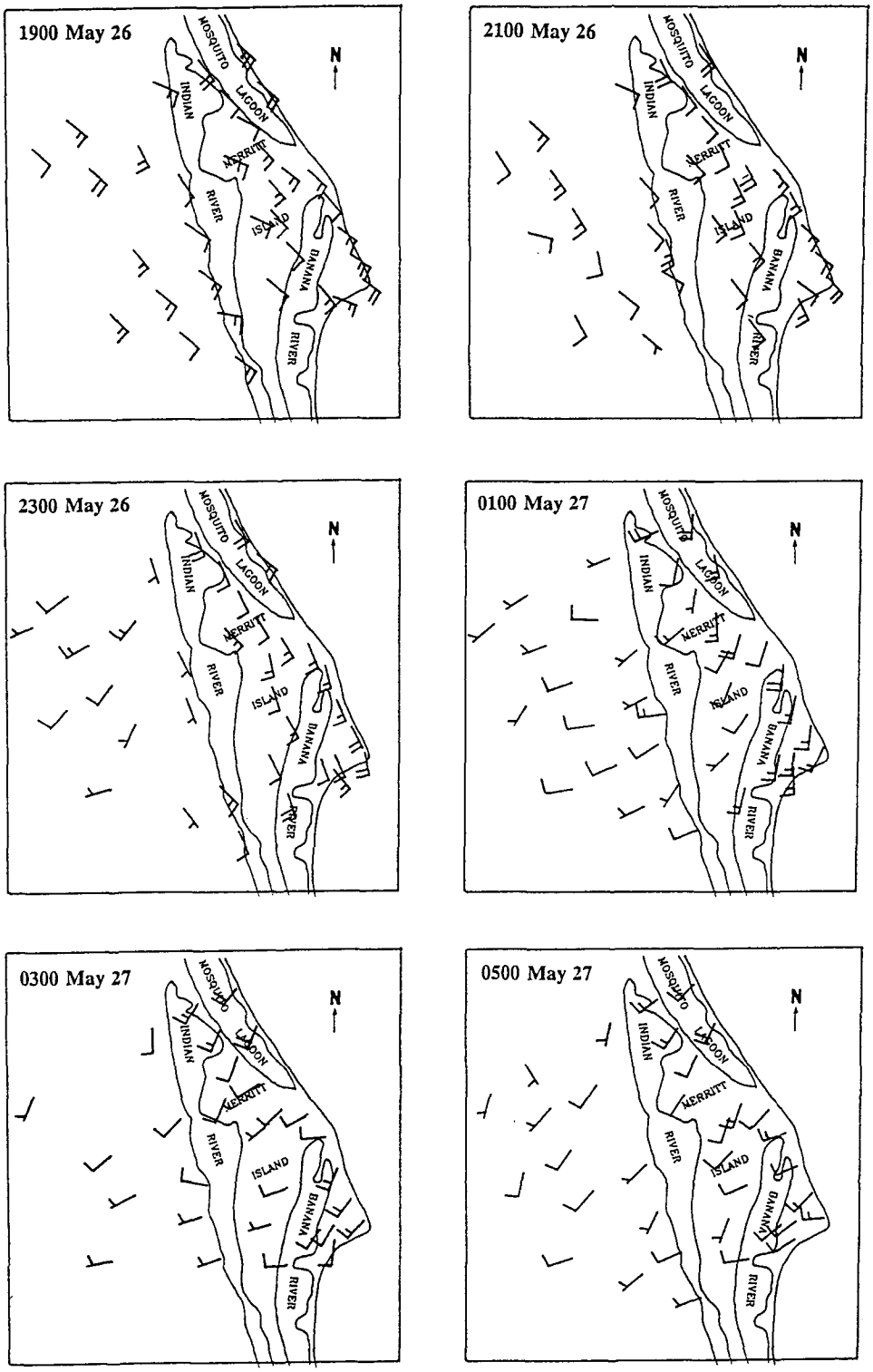

FIG. 5. (*Continued*)

merged. The speed of the sea-breeze front on this day over Merritt Island was greater in the northern and southern parts of the island than in its central part, as also was observed (Taylor et al. 1990) and simulated (Zhong et al. 1991) during the fall season. The reason for this may have been the location of Mosquito La-

goon to the north and Banana River to the south, which acted to speed up the sea-breeze front because the water surface was smoother and cooler than the land surface, thereby presenting less resistance to the airmass movement.

One notable feature in the daytime wind regime was that wind speeds increased as the surface heating increased and reached a maximum speed of 6 m s^{-1} between 1400 and 1500 when the temperature contrast between land and water reached its maximum. Another notable feature was that wind speed decreased markedly with distance inland, so that the strongest winds in the entire area always occurred at the coast. These features agree with both linear theory (Walsh 1974) and other observations (Hsu 1970; Raynor et al. 1979).

The nighttime regime began at sunset, as indicated by a wind-direction change at 1900 from onshore to southeasterly parallel to the shore. As the cooling reversed the land–water temperature contrast, the winds turned offshore. The wind-vector rotation was particularly rapid and accompanied by a slight decrease in wind speed between 2200 (not shown) and 2300 in the inland area west of the Indian River and between 2300 and 0000 (not shown) over Merritt Island. There was little change in either wind direction or speed during the remaining nighttime hours, suggesting that a quasi-steady state had been reached.

Figure 6 shows hodographs of the hourly wind vectors at 16.5 m measured by towers 0005 (near the coast), 0509 (at the center of Merritt Island), and 1605

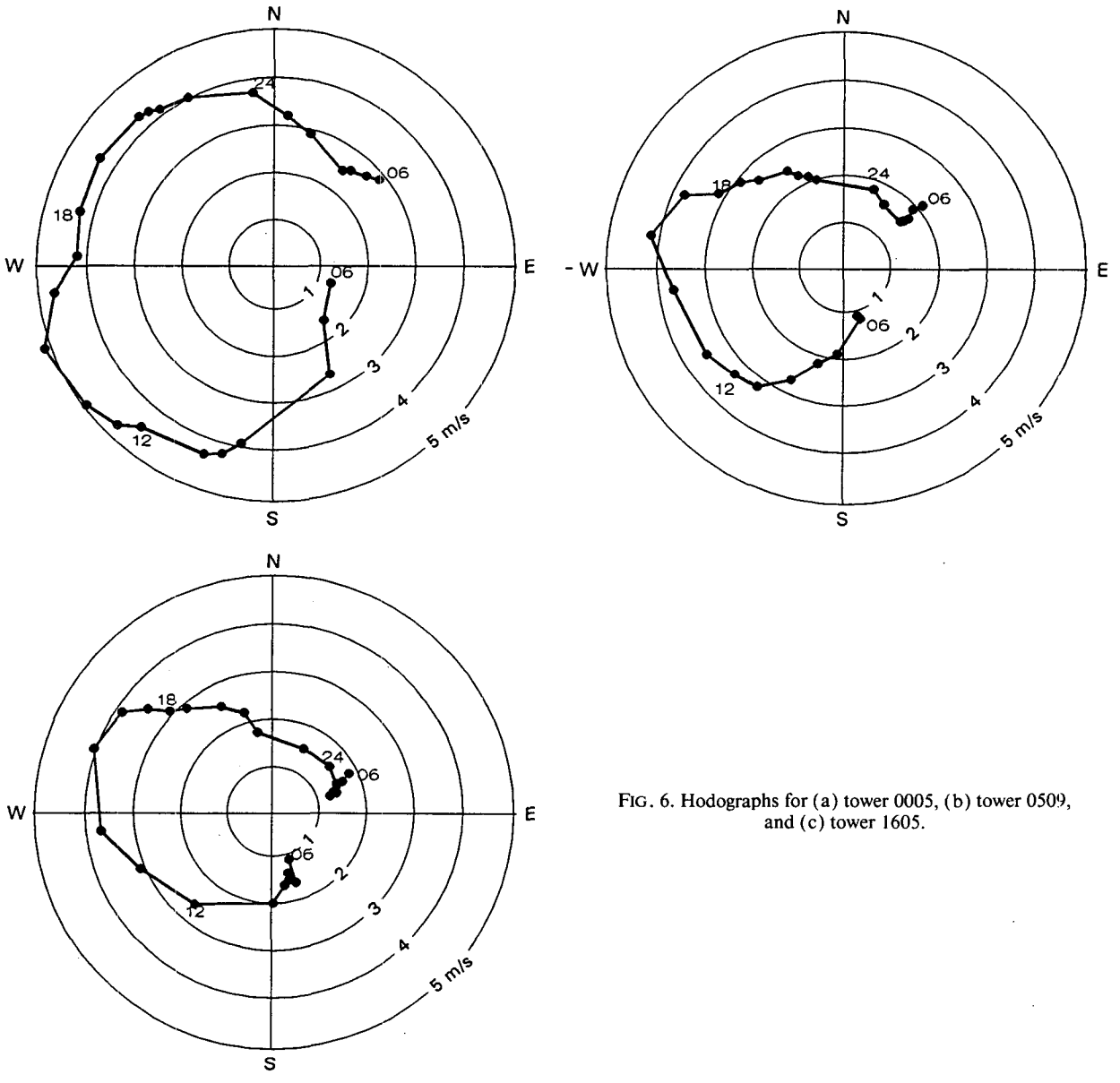

FIG. 6. Hodographs for (a) tower 0005, (b) tower 0509, and (c) tower 1605.

(west of the Indian River), which reveal the evolution of the low-level wind vector over the diurnal cycle in the areas surrounding these towers. The usual veering of the midlatitude sea–land breeze was clearly evident at all three locations. The rate of the rotation at each location, however, was far from uniform over the diurnal cycle. A common feature at all three towers was a rapid rotation during the daytime (especially in the afternoon hours), a slow turning in the evening, and another rapid rotation around midnight, followed by a quasi-steady state for the 3–5 h before sunrise. The rotational rates at any given time also were different from tower to tower. These features indicated that the forcing responsible for the rotation was not uniformly distributed in either time or space, which is consistent with Neumann's (1977) linear theory. Neumann showed that although the Coriolis force is the fundamental physical factor causing the usual clockwise turning of the midlatitude sea–land breezes, interactions between the mesoscale and large-scale pressure-gradient forces and the breezes, which are variable in both space and time, modify the rotational rate to create nonuniform turning of the wind. Burk and Staley (1979) pointed out that friction has a significant effect on rotation of the wind vector, a factor not explicitly included in Neumann's formulation. Kusuda and Abe (1989) recently showed that the effect of horizontal advection on rotation of the wind vector also can be comparable to the Coriolis force in a limited area.

A detailed analysis of the rate of rotation was impossible from the KABLE data because it is very difficult to get accurate values of such factors as pressure gradients, which are needed to estimate individual terms in the equation for the rotation rate (Neumann 1977). An order-of-magnitude estimate using the tower data indicated that over most areas of KSC–CC the mesoscale and large-scale interaction terms usually had different sign and had an order of magnitude that was comparable to the Coriolis term. Horizontal advection occasionally had the same magnitude in some areas at KSC–CC. The rate of rotation depends on the balance of all forces in a quite complex way, which can only be examined in detail by numerical modeling.

It is also evident in Fig. 6 that the wind speeds at tower 0005 near the coast are always much larger than those at the other two locations, which agrees with the conventional view that the wind speed in the sea–land-breeze layer decreases with inland distance as a result of the increase in friction and the decrease in the horizontal temperature gradient inland from the shore.

We plotted in Fig. 7 the time rate of change of temperature, dewpoint, and wind barb at Orlando International Airport (90 km inland) to determine the inland penetration after the sea-breeze front passed the entire tower network. A sharp shift in wind direction was observed between 1700 and 1800, along with an abrupt increase in dewpoint and a slight decrease in temperature. This suggests that a relatively humid, cool

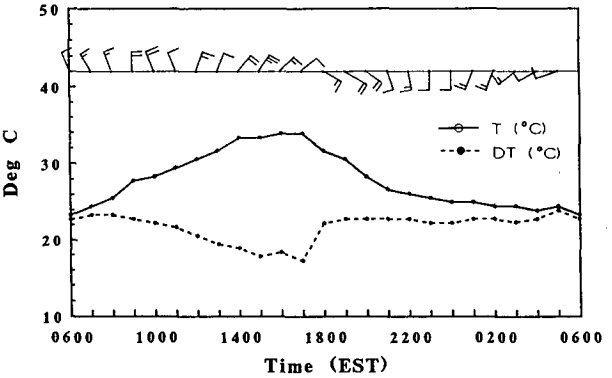

FIG. 7. Diurnal evolution of temperature, dewpoint, and wind at station MCO.

air mass moved past the station as the sea breeze penetrated farther inland. The average speed of the sea-breeze frontal movement after it passed the westernmost tower at about 1500 was estimated to be 4–6 m s^{-1}, which was more than twice the average speed of the sea-breeze front in the previous time period when it was passing the KSC–CC area. Acceleration of the sea-breeze front inland movement in the late afternoon also was observed by Simpson et al. (1977).

Seaward expansion of the sea-breeze circulation cell is illustrated in Fig. 8, where we have plotted the time history of wind data from coastal data buoy 41009 (about 40 km offshore). The wind at the data buoy 41009 turned onshore quite abruptly just after 1300, indicating the influence of the sea-breeze circulation. At the same time, the sea-breeze front measured by the tower network reached the west bank of the Indian River, which is about 20 km inland. Therefore, the sea-breeze circulation cell was not symmetric with respect to the coastline but extended offshore twice as far as onshore. Although one offshore data location is insufficient to track the sea-breeze boundary, asymmetry of the sea-breeze circulation cell has been found in other sea-breeze studies. Chang et al. (1982) showed in their two-dimensional numerical simulation that after 7 h of surface heating without synoptic forcing, the sea-breeze circulation reached about 20 km inland and 35 km offshore (Fig. 9). Arritt (1988) showed from a three-dimensional numerical model that the seaward extension of the sea-breeze circulation is about twice the landward extension. These numerical results are consistent with the observations presented here. A comparison of Fig. 8 with Fig. 6 reveals a different nighttime behavior between the wind rotation over the Gulf Stream and over the land. A larger rotation rate over the ocean indicates the dominance of the Coriolis force over the mesoscale pressure-gradient force, friction, and advection, which were all quite small over the ocean compared to those over land.

Figure 10 shows rawinsonde profiles of cross-shore

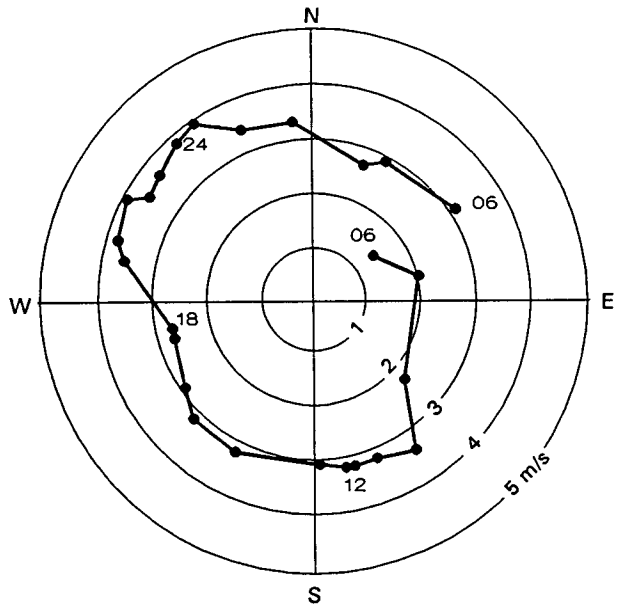

FIG. 8. Hodograph for data buoy 41009.

wind components at 2-h intervals. The daytime profiles show sea-breeze onshore flow in the low levels and offshore return flow aloft, and the nighttime profiles show the opposite. The depth of the sea breeze was 500–600 m before 1300, increasing to about 1 km at 1500, and then decreasing to about 800 m at 1700. The upper-level return flow was deeper than the sea-breeze layer but of weaker intensity, a result required by continuity. Land-breeze circulations driven primarily by mesoscale pressure gradients are usually shallower than sea-breeze circulations because there exists no low-level heat

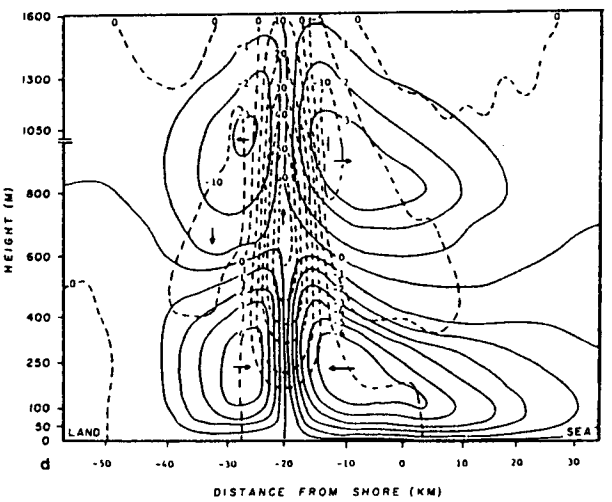

FIG. 9. Computed u (m s^{-1}, solid line) and w (cm s^{-1}, dashed line) for the calm synoptic case after 7 h of surface heating. From Chang et al. (1982, Fig. 4d).

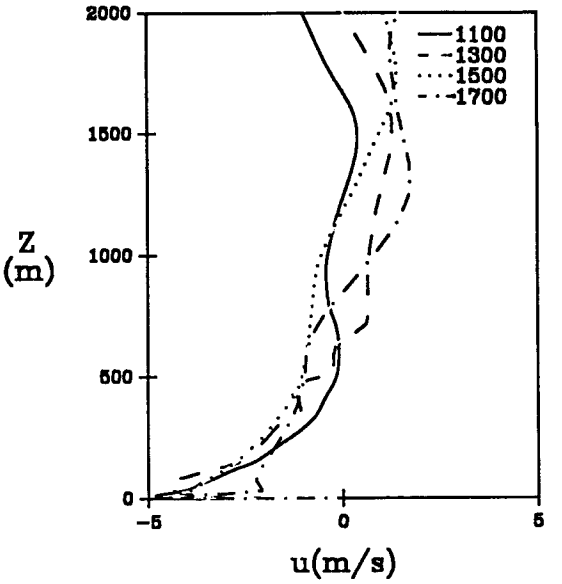

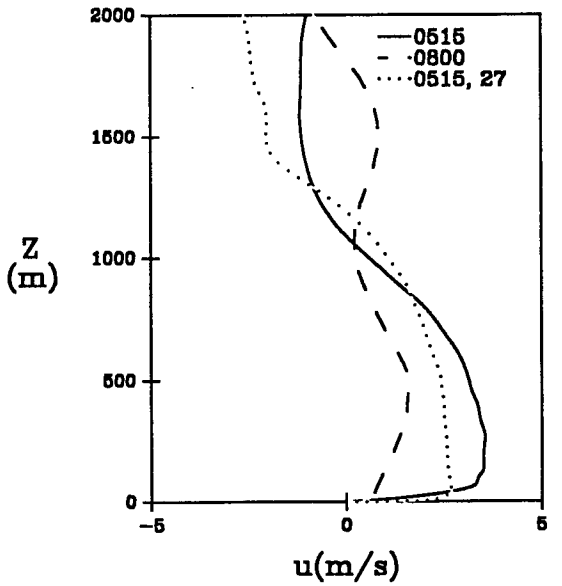

FIG. 10. Rawinsonde profiles of cross-shore wind component.

source to carry the circulation to greater height as with the sea-breeze circulation. For the present case, however, the depth of the land breeze was over 1 km. Comparison of the daytime (e.g., 1500) and nighttime (e.g., 0500) profiles shows that the speed of the sea breeze decreased rapidly with height, whereas the speed of land breeze decreased only modestly with height, further indicating that the energy source for the land breeze was not located at the surface as it was for the sea breeze. These features suggest that the mesoscale pressure gradient in a very shallow layer near the coast is much

less important in forcing the land breeze, compared with the sea breeze, over KSC–CC during this season. The Coriolis force, large-scale and mesoscale pressure gradient forces, friction, and advection effects (which can be large in this area) all likely contributed to the evolution of the land breeze.

Wind profiles from the LC39 sodar located near the beach and from the Jay-Jay sodar located near the west bank of the Indian River are plotted in Fig. 11. Both profiles show initial developments of the sea breeze and the IRB by about 0900 (keeping in mind that the shoreline is 333° at LC39 and about 350° at Jay-Jay). By 1100, the sea-breeze layer increased to about 360 m, while the IRB layer increased to about 260 m. As a result of noise problems, the LC39 sodar did not provide information at higher altitudes. The Jay-Jay sodar, on the other hand, indicated passage of the sea-breeze front at 1300 by an increase in both speed and depth of northeasterly onshore flow. The sea breeze continued throughout the day, and the depth of the

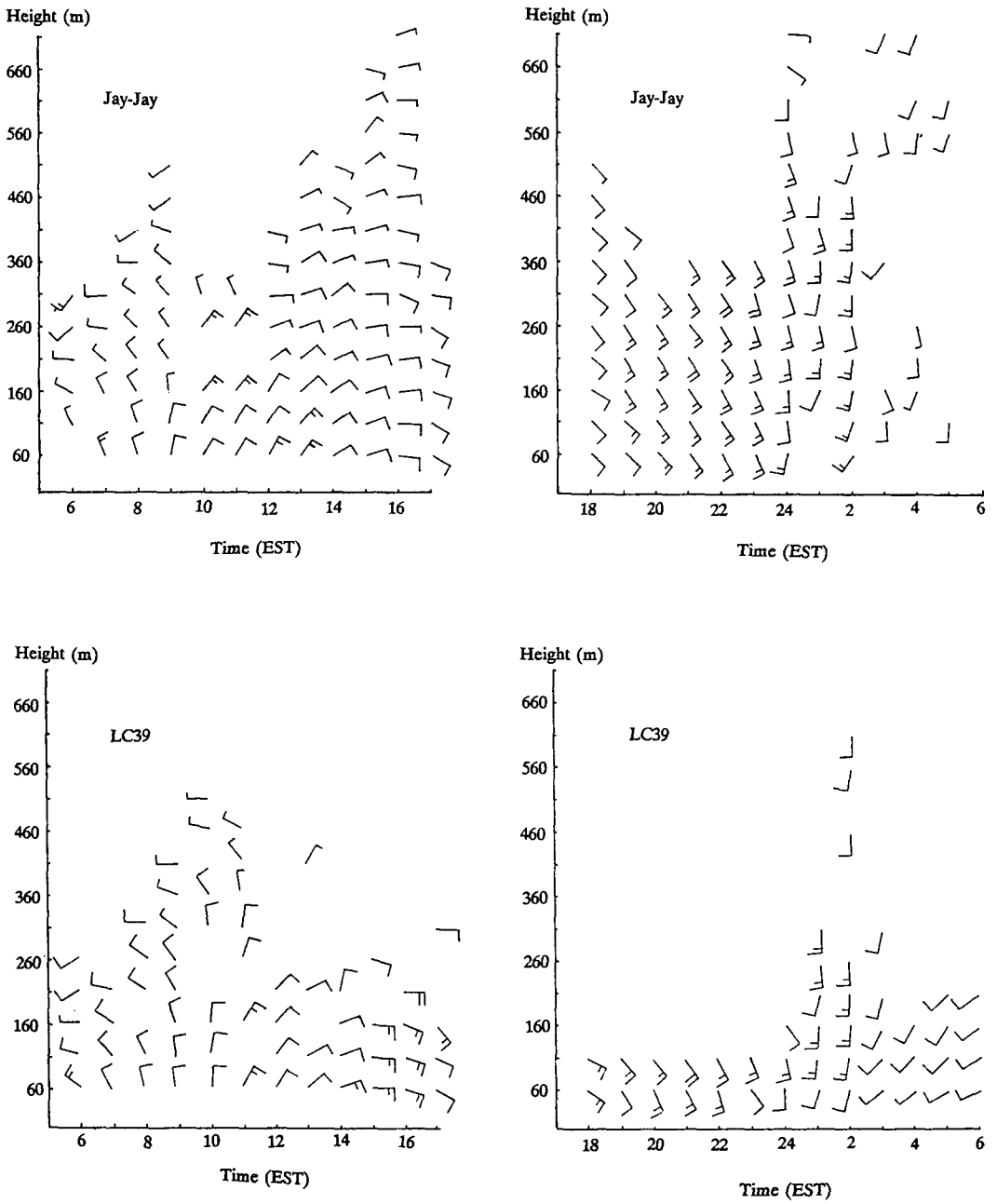

FIG. 11. Acoustic sounder wind profiles. Units: half-barb is 2 m s^{-1} and full barb is 4 m s^{-1}.

sea-breeze layer exceeded the upper limit of the observation so that the offshore return flow was not observed by the sodar. Winds at all levels veered with time, and the rates of turning were almost uniform in the lowest several hundred meters between 1300 (passage of the sea-breeze front) and 2300 EST (onset of the land breeze). A land breeze was observed throughout all levels after midnight and continued until the next morning. The speed of the land breeze was generally smaller than that of the sea breeze, a result of much weaker temperature contrasts at night compared with those during the daytime. Comparison of the profiles at the two sites showed that the wind speed at LC39 was always greater than that at Jay-Jay, which indicated greater thermal forcing and less friction near the coast.

c. *Thermal internal boundary layer*

A thermally induced local circulation can produce a thermal internal boundary layer (TIBL), which creates a potential for surface fumigation due to downward mixing of elevated pollutant plumes. Figure 12 shows the diurnal variation of the vertical potential temperature profiles measured by the rawinsonde. The arrows indicate mixing-layer heights, which correspond to the TIBL heights, approximated as the base of the inversion layer on the potential temperature profile. At 0515, a strong inversion existed throughout the boundary layer, thus indicating a stable atmosphere. After sunrise, the profile at 0800 showed that the surface inversion had been eroded by surface heating and replaced by a neutral to slightly unstable layer in the low level. The sea breeze moved into the rawinsonde site between 0900 and 1000 and confined the mixing to a shallow superadiabatic TIBL. The height of the TIBL was about 100 m at 1300, increased to 150 m by 1500, and then remained almost steady in the next few hours. The subsiding motion between return flow and the lower sea-breeze layer and the warm advection by the return flow were responsible for the warming in the region immediately above the TIBL and in the return flow layer, respectively. Mixing in the TIBL decreased after midday because of the weakening of surface heating. Development of the TIBL observed here is in good qualitative agreement with measurements obtained by Ogawa et al. (1985) as part of the Nanticoke II Shoreline Diffusion Experiment in Canada near Lake Erie. A possible explanation for the development of such a shallow TIBL was given by a reviewer who noticed the elevated mixed layer in the soundings between 1300 and 1700 EST in the region immediately above the TIBL. The reviewer suggested that a marine mixed layer of about 800-m depth probably was present over the warm Gulf Stream and might develop a shallow stable surface layer as it passed over cooler water near the coast. The marine mixed layer may have become decoupled from the surface as it penetrated inland. If the surface heating was sufficiently strong, it should be able to rapidly erode this decoupled marine mixed layer, in which case the TIBL would rapidly disappear and a mixed layer would be established throughout the depth of the sea-breeze layer. Unfortunately, no soundings were available farther inland and over the ocean to allow us to test this speculation. Numerical studies and possible future observations that include soundings farther inland might be able test this hypothesis. Description of the thermal structure in the land-breeze phase was hindered by a lack of nighttime temperature profiles, but the profile early the next morning showed a pattern similar to the profile at 0515 in Fig. 12, which indicated a radiative cooling throughout the night that generated a stable stratification. A survey of profiles taken on other days during the spring intensive data-collection period revealed that the evolution of the temperature profile in Fig. 12 is typical of diurnal pattern on days with sea-breeze development during the spring season. It needs to be pointed out that the evolution of the TIBL depth described by Fig. 12 was only for the rawinsonde location at Cape Canaveral Air Force Station, which is only about 3 km from the coast.

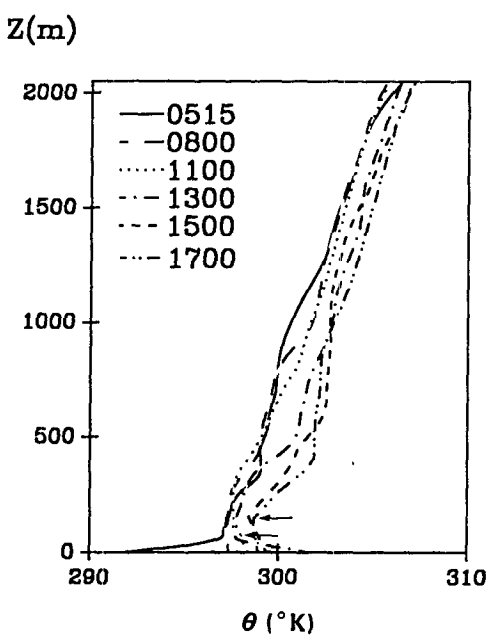

FIG. 12. Rawinsonde potential-temperature profiles.

d. *Turbulence and stability analysis*

Figure 13 shows the diurnal variation of the standard deviation of wind direction (σ_θ) from tower 0509, which was located at the center of Merritt Island about 9 km onshore, and from the near-shore (LC39) acoustic sounder. In the early morning, the PBL was stable over KSC–CC, as has been indicated by a strong surface inversion in Fig. 12. The wind was quite steady, with the

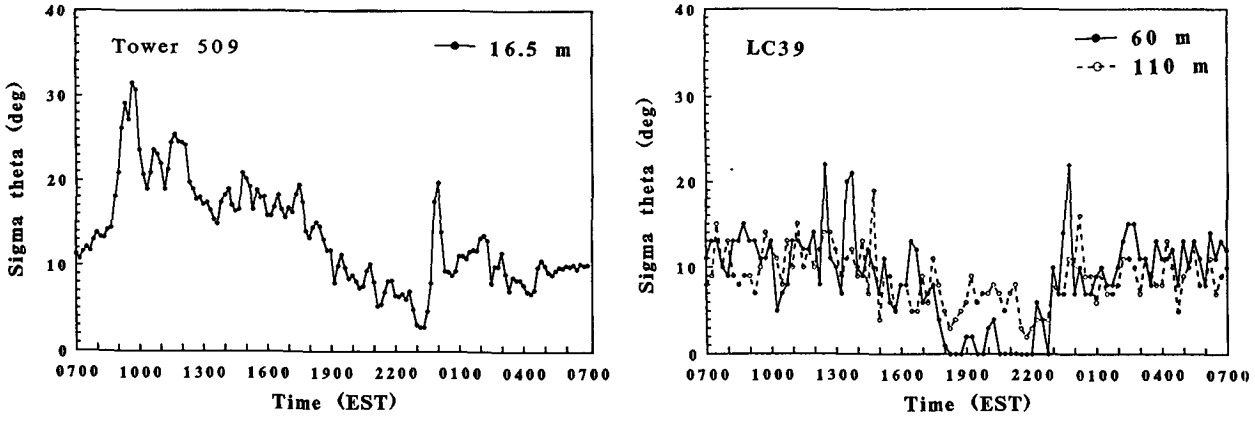

FIG. 13. Diurnal variation of standard deviation of wind direction at (a) tower 0509 and (b) LC39.

σ_θ value being about 10°. As the atmosphere started to warm up, σ_θ began to increase, confirming a change from stable to unstable stratification. Around 1000 EST, σ_θ peaked at 32°, indicating the beginning of a transition period during which the sea-breeze front passed the center of Merritt Island and was progressing westward across the KSC–CC area. The σ_θ value dropped after the frontal passage but remained relatively high and uniform in the afternoon, representing an unstable atmosphere caused by surface heating. After sunset at 1910, the σ_θ value gradually decreased to below 10°, which indicated that the lower atmosphere was stabilizing. An unexpected feature in this plot was a second peak just before midnight. Comparison with Fig. 5 shows that this is the time at which the land breeze reached tower 0509. As occurred at sea-breeze frontal passage, the σ_θ value dropped after transition to the land breeze and remained relatively steady until the next morning. The turbulence level was higher after midnight, possibly because the air mass brought into the area by the land breeze had a long inland trajectory and hence was not as stable as the previously existing marine air mass.

The σ_θ values measured at night by the sodar at coastal site LC39 were similar to those observed at tower 0509; the daytime values, however, were quite different. There was no peak in the σ_θ value associated with the sea-breeze frontal passage. This may have been a result of the sea-breeze front's passing over the LC39 sodar site about 2 h earlier than it passed tower 0509 and occurring when surface heating was weak and the sea breeze was at its initial development stage. The σ_θ values remained between 10° and 15° from sunrise to sunset, except for two peaks in the early afternoon when the heating was strong. Between sunset and midnight, the σ_θ value became quite small and showed characteristics of intermittent turbulence. After midnight, turbulence at the coast was very similar to that near the center of the island, with the σ_θ value peaking at the time when the land-breeze front passed the location and remaining large for the rest of the night. The average value of σ_θ in the land-breeze layer was, as expected, smaller than that in the sea-breeze layer near the center of the island, but the values were comparable at the coast. This was likely because instability during the daytime decreased toward the shore so that turbulent mixing near the shore was weaker than inland. The increase of instability with inland distance also was observed by Raynor et al. (1979) over Long Island. The amplitude of turbulent mixing at LC39 was larger at 60 m than at 110 m, except during the transition period between 1900 and 2200 when surface stabilization began.

5. Summary and conclusions

Data from the KABLE field experiment were used to characterize flow and temperature structure in the PBL over the KSC–CC area. In the case of a weak synoptic wind, the daytime flow structure was determined primarily by the local mesoscale pressure-gradient force created by the temperature contrast between land and water interfaces. A sea-breeze circulation, the dominant feature of the daytime flow field, was modified by a local river breeze, known as the Indian River breeze, in that diverging flow over the river enhanced convergence over Merritt Island and also generated a convergence zone west of the Indian River. The Banana River and Mosquito Lagoon also affected the flow structure by enhancing convergence in surrounding areas, and were responsible for a nonuniform inland movement of the sea-breeze front over Merritt Island. The sea-breeze layer extended upward slightly more than 1 km, and the Indian River breeze layer was deeper than 250 m. The average speed of sea-breeze inland penetration was 2 m s^{-1}, about twice the speed of the IRB, in the area of KSC–CC, and increased up to 4–6 m s^{-1} farther inland. The sea breeze penetrated more than 90 km inland from the coast. Although offshore data were limited, the sea-breeze circulation cell

apparently was not symmetric with respect to the coastline, with the seaward extension about twice the landward extension. A TIBL developed after onset of the sea breeze as a result of surface heating of the invading stable marine air. The height of this TIBL increased with time and reached a maximum of about 200 m between 1500 and 1600. The nighttime flow field was dominated by a land breeze. The local mesoscale pressure-gradient force was not the dominant force generating the land breeze, because the temperature contrast was quite weak throughout the night. The wind vector rotated at an irregular rate until midnight, after which time it assumed a relatively steady direction. In contrast to the daytime regime, which was forced primarily by the land–water temperature difference, the nighttime regime was forced by a changing combination of the Coriolis force, mesoscale and large-scale pressure-gradient forces, frictional force, and advection. Land–water temperature contrasts were so small at night that no clear convergence patterns associated with the rivers were observed. Measurements of standard deviations of wind direction (σ_θ) revealed an abrupt increase and then decrease in the low-level turbulence associated with passage of the sea-breeze front over Merritt Island. A peak also was observed before onset of the land breeze. Turbulent mixing remained relatively large in the land-breeze layer at night, especially near the coast, where nighttime turbulent mixing associated with the land breeze was almost comparable to daytime turbulent mixing.

Lack of upper-level observations prevents us from describing details of PBL structure at upper levels. It would be quite useful to know the horizontal distribution of upper-level wind and temperature fields, as well as the slope of the sea-breeze front and of the TIBL, which is a key factor for diffusion studies. It also would be useful to examine the spatial and temporal distribution of the forcing that may be responsible for the observed behavior of the flow system in this region. We were not able to separate these mechanisms with the data we had available. We have used a three-dimensional mesoscale model to study these questions and have attempted to interpret some of the observed phenomena described in this study. Results from the numerical study will be presented in a future report.

Acknowledgments. We are very grateful to Dr. G. E. Taylor and to Dr. M. K. Atchison of ENSCO Inc. for providing the KABLE data and for useful discussions that have made this study possible. Extensive comments by reviewers of the first draft led us to additional analysis and a better understanding of complexities of this flow field. We also greatly appreciate many fruitful discussions with Dr. R. Arritt. Partial support for this research was provided by DOE Grant W7405 EN682 under the CHAMMP initiative.

REFERENCES

Arritt, R. W., 1988: Numerical modeling of the offshore extent of sea breezes. *Quart. J. Roy. Meteor. Soc.*, **115,** 547–570.

Burk, S. D., and D. O. Staley, 1979: Comments "On the rotation rate of the direction of the sea and land breezes." *J. Atmos. Sci.*, **36,** 369–371.

Chang, L. P., E. S. Takle, and R. L. Sani, 1982: Development of a two-dimensional finite-element PBL model and two preliminary model applications. *Mon. Wea. Rev.*, **110,** 2026–2037.

Hill, K., 1967: Study of the land and sea breeze regions at Cape Kennedy, Florida from May 23 through September 1966. NASA/Marshall Space Flight Center Branch Memo., R-AERO-YE-29-67, 22 pp.

Hsu, S. A., 1970: Coastal air circulation system: Observations and empirical model. *Mon. Wea. Rev.*, **98,** 497–509.

Kusuda, M., and N. Abe, 1989: The contribution of horizontal advection to the diurnal variation of the wind direction of land–sea breezes: Theory and observation. *J. Meteor. Soc. Japan,* **67,** 177–184.

Lyons, W. A., D. A. Moon, J. A. Schuh, C. S. Keen, L. E. Newman, T. E. Nelson, R. A. Pielke, W. R. Cotton, R. Arritt, and R. G. Fisher, 1988: Conducting a "field program" on the southeast Florida coastline using a mesoscale numerical model. *Fourth Conf. on Meteorology and Oceanography of the Coastal Zone,* Anaheim, CA, Amer. Meteor. Soc., 107–110.

Neumann, C. J., 1971: The thunderstorm forecasting system at the Kennedy Space Center. *J. Appl. Meteor.*, **10,** 921–936.

Neumann, J., 1977: On the rotation rate of the direction of sea and land breezes. *J. Atmos. Sci.*, **34,** 1913–1917.

Ogawa, Y., T. Ohara, S. Wakamatsu, P. G. Diosey, and I. Uno, 1985: Observation of lake breeze penetration and subsequent development of the thermal internal boundary layer for the Nanticoke II Shoreline Diffusion Experiment. *Bound.-Layer Meteor.*, **35,** 207–230.

Raynor, G. S., S. Sethuraman, and R. M. Brown, 1979: Formation and characteristics of coastal internal boundary layers during onshore flows. *Bound.-Layer Meteor.*, **16,** 487–514.

Reed, J. W., 1979: Cape Canaveral sea breeze. *J. Appl. Meteor.*, **18,** 231–235.

Simpson, J. E., D. A. Mansfield, and J. R. Milford, 1977: Inland penetration of sea-breeze front. *Quart. J. Roy. Meteor. Soc.*, **103,** 47–76.

Taylor, G. E., M. K. Atchison, and C. R. Parks, 1990: The Kennedy Space Center Atmospheric Boundary Layer Experiment. Report No. ARS-90-120, ENSCO, Inc., Melbourne, FL, 229 pp.

Walsh, J. E., 1974: Sea breeze theory and applications. *J. Atmos. Sci.*, **31,** 2012–2026.

Zhong, S., J. M. Leone, Jr., and E. S. Takle, 1991: Interaction of the sea breeze with a river breeze in an area of complex coastal heating. *Bound.-Layer Meteor.*, **56,** 101–139.